JOURNAL OF ENGINEERING SCIENCES

Volume 13, Issue 1 (2026)

Obertyukh R., Slabkyi A., Povstyanoy O., Bakalets D., Polishchuk V. (2026). Mathematical modeling of a small-dimension hydropulse vibrator with a valve-driven pressure pulse generator. Journal of Engineering Sciences (Ukraine), Vol. 13(1), pp. F1–F16. https://doi.org/10.21272/jes.2026.13(1).f1

p-ISSN 2312-2498
e-ISSN 2414-9381

Mathematical Modeling of a Small-Dimension Hydropulse Vibrator with a Valve-Driven Pressure Pulse Generator

Obertyukh R.[1][0000-0003-2939-6582], Slabkyi A.[1][0000-0001-9284-2296], Povstyanoy O.[2*][0000-0002-1416-225X], Bakalets D.[1][0000-0003-1528-2066], Polishchuk V.[1][0009-0000-0293-8711]

[1] Vinnytsia National Technical University, 95, Khmelnytske Hwy., 21021, Vinnytsia, Ukraine;
[2] Lutsk National Technical University, 75, Lvivska St., 43018, Lutsk, Ukraine

Article info:
Submitted: November 6, 2025
Received in revised form: March 21, 2026
Accepted for publication: March 26, 2026
Available online: April 1, 2026

***Corresponding author:**
povstjanoj@ukr.net

Abstract. The article presents research on a new compact vibrator design based on a hydraulic pulse drive with a built-in valve-type pressure pulse generator. Based on scientific assumptions, an approximate cycle diagram of the working cycle, a structural diagram of the vibrator, and a representation of the hydraulic link of its hydraulic system as a Kelvin–Voigt model were developed. A dynamic model of the vibrator was designed, in which the hydraulic link interacts with the moving links via transmission ratios. Based on simplified dynamic models of the forward and reverse strokes of the executive element, a mathematical model of the vibrator was developed using the d'Alembert principle, resulting in a system of 2nd-order differential equations describing the motion of the executive element's mass during its forward and reverse strokes. Consumption for energy equations at time intervals was also considered according to the approximate cycle diagram of the vibrator's working cycle and the conditions of uniqueness that limit the movement of the mass of the executive element and the deformation of the hydraulic link. To provide a detailed analysis of the developed mathematical model, Python program code was written. The workflow was visualized in Google Colab. It was confirmed that the operating frequency range of a hydraulic pulse vibrator of this design is not a single fixed number – it is parametric and depends on the settings of the hydraulic system. By adjusting the pumping station parameters and the stiffness of the vibrator's elastic elements, it is possible to achieve an actuator frequency up to 150 Hz and an amplitude of up to 2 mm.

Keywords: energy-efficient frequency control, optimized vibration amplitude, sustainable system modeling and simulation, hydraulic vibration drive.

1 Introduction

The intensification of industrial technological processes through the use of vibrations requires the development of new models of vibration equipment, particularly vibrators. The development of high-efficiency vibration systems is closely linked to advances in hydraulic pulse generation technologies.

Recent international research focuses on the transition from large-scale industrial vibrators to small-dimension high-frequency units, which require sophisticated mathematical modeling due to the increased influence of nonlinear fluid dynamics. The authors have developed a new design of a small-sized vibrator based on a hydraulic pulse drive (HPD) with a built-in valve-type pressure pulse generator [1]. First of all, it is advisable to study this construction using theoretical methods, in particular by mathematical modeling.

This article aims to develop and provide a scientific justification for a mathematical model of a compact hydraulic impulse vibrator with parametric valve control, enabling the optimization of its design parameters for effective use in vibration drives for various industrial applications, including vibratory rammers, surface strain hardening, and test benches.

2 Literature Review

The analysis of literature sources shows the relevance of mathematical modeling of vibration systems and the need to improve it, taking into account the peculiarities of the technological process, design, and vibration drive type [2, 3]. Highly efficient mathematical modeling will greatly accelerate the introduction of new equipment models. The research work [4] developed a hydraulic composite actuator for vibration modeling and proposed an iterative open-loop learning method to solve the control problem.

The research [5] focuses on the computer simulation and experimental testing of the improved vibratory screening conveyor equipped with a controllable crank-type exciter, characterized by variable forced frequency and eccentricity. The main scientific novelty of this research is the implementation of a three-mass discrete-continuous oscillatory system, in which the disturbing body is modeled as a flat spring with both inertial and stiffness parameters.

In the research work [6], the steady-state modes of motion of a single-mass resonant vibratory machine were defined and investigated for stability. The results reported here are applicable in the design of resonant single-mass vibratory machines with inertial vibration exciters of the ball, roller, or pendulum type.

The article [7] presents the synthesis of the design parameters of a two-frequency inertial vibrator based on the specified power characteristics. Based on the developed mathematical model, the parameters of the variable periodic force are derived for two angular velocities.

Recent studies by Zhu et al. [8] emphasize that valve-based generators offer superior control over wave amplitude compared to rotary systems, especially in drilling and material processing. Furthermore, the integration of fast-switching valves, as discussed by Gutierrez et al. [9] in the context of digital hydraulics, has opened new possibilities for generating precise pressure pulses by minimizing switching delays.

According to research, reducing the size of hydraulic vibrators makes the "scaling effect" a critical factor.

Al-Obaidi and Alhamid [10] demonstrated that in small-dimension hydraulic exciters, the viscous friction and internal leakages have a disproportionate impact on the exciter's frequency response. Their work uses lumped-parameter modeling to describe the interaction between the fluid and the mechanical actuator, a method highly effective for real-time control applications.

An HPD provides pressure feedback, which simplifies the vibration drive control system of various technological machines and provides a wide range of vibration loads with the possibility of independent adjustment of the amplitude and frequency of oscillations of the executive body of the technological machine. The peculiarities of the development and research of the HPD are described in other relevant works [11–15].

Modern mathematical models increasingly move away from simplified harmonic assumptions. The research work by Al-Obaidi and Alwatban [16] highlights the importance of accounting for fluid compressibility and the "effective bulk modulus" in small chambers, where even minor air entrainment can significantly dampen the vibration energy. Moreover, advanced computational fluid dynamics (CFD) and fluid-structure interaction (FSI) techniques, as demonstrated by Hua et al. [17], provide insights into pressure rise rates within valve chambers, which are crucial for optimizing the vibrator's impact force.

Despite these advancements, there is a lack of comprehensive models that simultaneously account for the nonlinear dynamics of a valve-type pressure pulse generator integrated with a small-scale vibration unit under varying load conditions.

The theory and methodology for calculating hydraulic impulse machines and devices are presented in the context of hydraulic impulse drives for specific vibration machine designs, whose mathematical models are based on dynamic models and structural calculation diagrams [11].

The mathematical model of an HPD is usually presented as differential equations of motion for the shut-off and distribution elements of its cascades, and as equations for the energy carrier flow distributed by the pressure pulse generator (PPG) during the working cycle [11–13]. To simplify the mathematical models of a hydraulic impulse drive, dynamic processes in the hydraulic impulse drive are sometimes neglected, considering the operation of the HPD to be instantaneous ("relay"), which, in our opinion, does not allow for an adequate description of the drive dynamics and is the cause of significant differences between the results of theoretical and experimental studies of the drive of vibrating machines, since the shape and characteristics of the pressure pulse are determined by the dynamic processes in the HPD and its design features.

In traditionally constructed mathematical models of PPG, the differential equations of motion of the shut-off and distribution elements of the cascades are the algebraic sum of the forces of inertia, motion, position (weight and elastic elements), and friction (dry and viscous). For the uniqueness of the solution of the system of differential equations of motion of the shut-off and distribution elements of the PPG, a system of equations of energy carrier flow through the corresponding passage cross-sections of the PPG is added to it, which, as a rule, consists of a first-order differential equation describing the law of pressure increase in the PPG system and equations of balance of flow between the cavities of the hydraulic impulse drive during the working cycle. The mathematical model also imposes certain restrictions on changes in the energy carrier pressure, strokes, and speeds of the shut-off and distribution elements of the HPD, etc., under conditions of uniqueness.

Simplified mathematical models describe the HPD operating cycle as a single-stage process, without distinguishing between separate phases [11–14], which, in our opinion, does not allow for an adequate reflection of the dynamics of the hydraulic impulse drive and the creation of correct methods for the design calculation of the HPD.

3 Research Methodology

3.1 Design modeling

The structural diagram of the vibrator is shown in Figure 1.

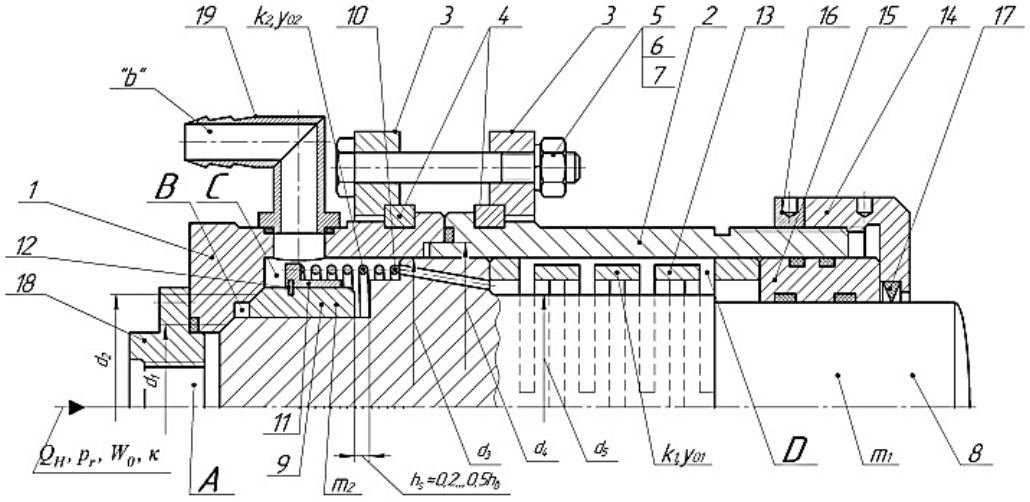

Figure 1 – Design scheme of a small-sized hydraulic pulse vibrator with a built-in valve pressure pulse generator: 1 – housing body; 2 – sleeve-hydraulic cylinder; 3 – flanges; 4 – half rings; 5 – bolts; 6 – nuts; 7 – spring washers; 8 – plunger; 9 – sleeve; 10 – twisted spring; 11 – stepped sleeve; 12 – spring ring; 13 – slotted spring; 14 – cap nut; 15 – cylindrical sleeve; 16 – nut; 17 – dirt remover; 18 – plunger rod; 19 – nipple (*A* – chamber; "*b*" – hole; *B* – intermediate chamber; *C* – drainage cavity; *D* – cavity; d_1, d_2 – average diameters, m; d_3, d_4, d_5 – structural diameters of the sleeve and plunger, m; h_s – gap, m; k_1 – stiffness of the slotted spring, N/m; m_1, m_2 – masses, kg; p_r – energy carrier pressure, Pa; Q_H – flow rate, m^3/s; W_0 – original volume, m^3; y_{01} – preliminary deformation of the slotted spring, m; y_{02} – pre-strain of the twisted spring, m; κ – effective bulk modulus, Pa)

The power link of the vibrator (the plunger hydraulic cylinder) consists of a body 1, fixed to the frame (base) of the plant, machine, etc. The body 1 is connected to the sleeve-hydraulic cylinder 2 of the vibrator by means of flanges 3, which are tightened through half rings 4 with bolts 5 and nuts 6, secured with spring washers 7.

Half rings 4 are installed in the recesses of the body 1 and the hydraulic cylinder sleeve 2.

The plunger 8 of the hydraulic pulse vibrator, in addition to the power function, is part of a single-stage parametric pressure pulse generator, since at the left end of the plunger 8, the first degree of sealing of the generator is formed by means of a valve chamfer at the end of this end of the plunger 8. This chamfer is in contact with the seat (lapped on it) along the average diameter d_1 formed in the bore of the body 1.

The second degree of sealing of the PPG is realized by the valve sleeve 9, which is mated by a lapped chamfer formed on its left end along the average diameter d_2 of the second seat made in the bore of the body 1, coaxially with the seat of the first degree of sealing of the PPG with an average diameter d_1.

The initial contact pressure on the mating surface of the lapped chamfers of the valve sleeve 9 and the seat of the second sealing stage of the PPG in the body 1 along the average diameter d_2 is provided by the force of the twisted spring 10, which acts on the valve sleeve 9 through the stepped sleeve 11 located on the outer surface of the valve sleeve 9 and the spring ring 12.

The slotted spring 13, which is installed in the cavity *D* formed between the central through bore in the hydraulic cylinder sleeve 2 and the plunger rod 8, rests with its left end against the right end of the guide part of the plunger 8 with a diameter of d_3, which is mated to the surface of the central through bore in the hydraulic cylinder sleeve 2.

To ensure alignment between the borings with a diameter of d_3 in the hydraulic cylinder sleeve 2 and the body 1, as well as with the conical chamfers of the seats of the locking elements of the first and second stages of sealing of the PPG, which are in contact, respectively, with the chamfers on the left ends of the plunger 8 and the valve sleeve 9, on the left end of the hydraulic cylinder sleeve 2 there is a cylindrical projection with a diameter of d_4, which is mated to the surface of the blind bore in the housing 1, and the right end of the housing 1 rests against the left end of the hydraulic cylinder sleeve 2, which is an additional centring surface of the body 1 relative to the hydraulic cylinder sleeve 2.

The outer surfaces of the resistance guide the slotted spring 13 rings along the diameter d_3 to the surface of the hydraulic cylinder sleeve 2.

A gap is formed between the outer surfaces of the working rings of the slotted spring 13 and the surface of the hydraulic cylinder sleeve 2 with a diameter of d3, which requires jamming of the slotted spring 13 during the stroke of the plunger 8 [17, 18].

Adjustment of the preliminary deformation y_{01} of the slotted spring 13 is carried out by means of a cap nut 14,

which, through a cylindrical sleeve 15, which is mated along the running seats in diameter d_5 with the surface of the plunger outlet ring 8 and the surface of the through central bore with a diameter d_3 of the hydraulic cylinder sleeve 2, interacts with the right (according to Figure 1) end of the slotted spring 13 support ring. The cap nut is secured with nut 16.

For diameters d_3 and d_5, the bushing 15 is sealed with O-rings. The surface of the plunger outlet ring 8, with a diameter d5, is protected from environmental contamination by a dirt remover 17 installed in the bore of the union nut 14.

The choice of a slotted spring 13 instead of a standard coil spring is dictated by the need to ensure high specific stiffness and minimal inertial mass within the strict dimensional constraints of the vibrator's internal cavity, which is critical for maintaining stable vibrations at frequencies up to 150 Hz. To achieve a frequency of up to 150 Hz, the system requires high stiffness k_1. A helical spring with equivalent stiffness would have significantly larger dimensions (diameter and length), which would make it impossible to fit within cavity *D* between the housing and the plunger rod 8. The slotted spring design ensures better centering of the plunger 8 and prevents misalignment during rapid strokes h_p.

In order to clearly implement the parametric principle of opening and closing the locking elements of the first and second stages of the PPG sealing, a gap $h_s = (0.2–0.5)\cdot h_b$ is formed between the right end of the sleeve-valve 9 and the left end of the plunger guide part with a diameter of d_3, where h_b – the negative overlap (opening) of the second stage of the PPG sealing.

The drainage cavity *C* of the vibrator is connected to the hydraulic tank of the hydraulic pumping station via the angular nipple 19, installed in hole "b" and freely connected to the drainage cavity *C*. The pre-strain y_{02} of the twisted spring 10 is provided during the connection of the body 1 and the hydraulic cylinder sleeve 2.

The opening of the PPG valve begins when the pressure in the pressure chamber *A* reaches the PPG opening pressure [19]:

$$p_A = p_{1max} \geq \frac{k_1 y_{01} + F_{T0}}{A_1}, \quad (1)$$

where k_1 – stiffness of the slotted spring, N/m; F_{T0} – the initial force of the technological resistance of the object under technological influence of the plunger rod 18, which may be constant or variable, depending on the type of technological vibration process being implemented.

In the case of vertical placement of the vibrator F_T, the weight of the technological object and the attached (or combined with it) masses m_{max} should be determined as $F_G = m_{max}\cdot g$, where here $g = 9.81$ m/s^2 – gravity acceleration; A_1 – the average cross-sectional area of the sealing element of the first sealing stage of the PPG, m (Figure 1).

Once the chamfer of the sealing element of the first sealing stage of the PPG has been disengaged (marking the start movement of the plunger 8), chamber *A* and intermediate chamber *B* are connected, and the pressure of the working fluid within them is balanced almost instantly at the level p_{1max}, due to the small volume of chamber *B*.

Under the action of this working fluid pressure, the valve sleeve 9, overcoming the resistance of the twisted spring 10, lifts off its seat, moves rapidly along the gap h_s, adjusts with its right end against the left end of the guide section of the plunger 8 with diameter d_3 and then moves with it until the PPG is fully open to its working stroke $h_p \geq h_b$.

The contact pressure required for sealing in the initial position of the valve sleeve 9 can be calculated as follows:

$$p_c = \frac{4k_2 y_{02}}{\pi d_2^2} \approx 1.274 k_2 y_{02}, \quad (2)$$

where k_2 – the stiffness of the twisted spring, N/m.

Due to the opening of the PPG, the pressure chamber *A* and drainage cavity *C* are connected through the nipple 19 to the tank of the hydraulic pumping station, and the pressure level of the energy carrier in the hydraulic system of the vibrator (including, in addition to the vibrator, the hydraulic pumping station) begins to decrease. For the locking element of the second sealing stage of the PPG, the pressure of the energy carrier can be reduced to the following level:

$$p_A \leq p_{2max} \leq p_{1max}\left(\frac{d_1}{d_2}\right)^2 + \frac{k_1 h_p + F_{Tmax} + k_2(y_{02} + h_S)}{A_2}, \quad (3)$$

where F_{Tmax} – maximum resistance force of a technological object, N; A_2 – average cross-sectional area and valve sleeve 9, m^2;

During this reduction, reverse stroke h_{rev} of the plunger 8 occurs with the valve sleeve 9 ($0 \leq h_{rev} \leq h_p$).

The maximum vibration frequency of the plunger 8 is equal to the maximum frequency of pressure pulses with a theoretical amplitude $\Delta p = (p_1 – p_2)$, which the vibrator's PPG does not control, determined by the design parameters of the PPG, mainly by the ratio d_1/d_2, the value of the supplied energy carrier flow, usually the flow rate Q_H of the pump of the hydraulic pumping station of the vibrator's hydraulic system, and the effective bulk modulus κ of the energy carrier.

To ensure high reliability and minimize mechanical energy losses at operating frequencies up to 150 Hz, the sealing between the plunger 8 and the valve sleeve 9 is designed as a precision gap seal (non-contact type). The radial clearance in this coupling is maintained at 5–10 μm, effectively limiting volumetric leakage. In the developed mathematical model, these minor leakages are integrated into the overall flow coefficients and the effective bulk modulus of the energy carrier.

This approach allows the hydraulic line (HL) to be represented as a Kelvin–Voigt viscoelastic body, where the dissipative component c_0 accounts for both internal fluid friction and pressure drops due to microleakages.

Given the high rate of pressure rise and the parametric nature of the pulse generation, such localized leakages do not significantly distort the pressure pulse shape or the stability of the auto-oscillatory process, while their influence on the system's static stiffness is reflected in the corrected effective bulk modulus κ.

Usually, the operating cycle of a hydraulic pulse vibration drive (VD) and a vibration-impact machine (VIM) and devices can be divided into separate phases [15], which, in order to simplify their mathematical description, are combined into forward and reverse strokes of the executive links of the PPG and power links of hydraulic motors (hydraulic cylinders). It is advisable to take the end planes of the sealing chamfers of the plunger 8 (the first stage of sealing of the PPG) and the valve sleeve 9 (the second stage of sealing of the PPG) as the starting point for the forward and reverse strokes (Figure 1), respectively: y_{1F}, y_{1rev}; y_{2F}, and y_{2rev}, where indices "*F*" and "*rev*" mean forward and reverse strokes, respectively).

In the dynamic process of the vibrator's operating cycle, the combined masses are moved:

$$m_1 = m_8 + m_{13};$$
$$m_{13} = 2\pi Rna^2\rho + 2a^3(n+1)\rho + 6\pi Ra\rho; \quad (4)$$

$$m_2 = m_9 + m_{10} + m_{11} + m_{12}, \quad (5)$$

where m_i – mass of the i-th element presented in Figure 1, kg; a – jumper's edge, m; ρ – material density, kg/m^3; n – number of jumpers.

3.2 The working cycle description

The working cycle of the hydro-pulse vibrator, assuming the cycle during the forward and reverse strokes of masses m_1 and m_2, can be described as an oriented cyclogram of the first two pulses of pressure change p_r (Figure 2, curve 1) in the pressure cavity A (Figure 1) and displacement y_1 (Figure 2, curve 2) of mass m_1, as well as displacement y_2 of mass m_2, without taking into account transient processes in actual HPDs and devices during their start-up and is repeated to a certain extent in the successive operating cycles of these machines.

Friction forces cause transient processes during the movement of the moving masses of the PPG and the actuators of the VD and VIM, the influence of dissolved air and temperature on the physical and mechanical properties of the energy carrier, which change such physical parameters of the energy carrier as its density ρ_e, elastic modulus κ, dynamic viscosity $\mu_e = \nu_e \cdot \rho_e$, where ν_e – kinematic viscosity of the carrier, m^2/s.

The influence of the mentioned factors on the working process of hydraulic pulse machines can be assessed only from experimental results.

The stable mode of operation of the vibrator is characterized by the same periods T_T of pressure change p_r, displacements y_1 and y_2 (respectively T_K and T'_K), which are the sum of the corresponding time intervals (Figure 2):

$$T_T = t_H + t_{BT} + t_{rT} + t_{HT} = \\ = T_K = t_{kn} + t_{kb} + t_{RS} + t_{kh} = \\ = T'_K = t'_{kn} + t'_{kb} + t'_{RS} + t'_{kh}, \quad (6)$$

where t_H – the time of the energy carrier pressure rise from p_2 to p_1 in the pressure cavity A of the vibrator, s; t_{BT} – the time of pressure reduction from p_1 to p_2 in the pressure cavity A during the opening of the PPG shut-off elements, s (here p_1, p_2 – opening and closing pressure levels of the pressure pulse generator, Pa).

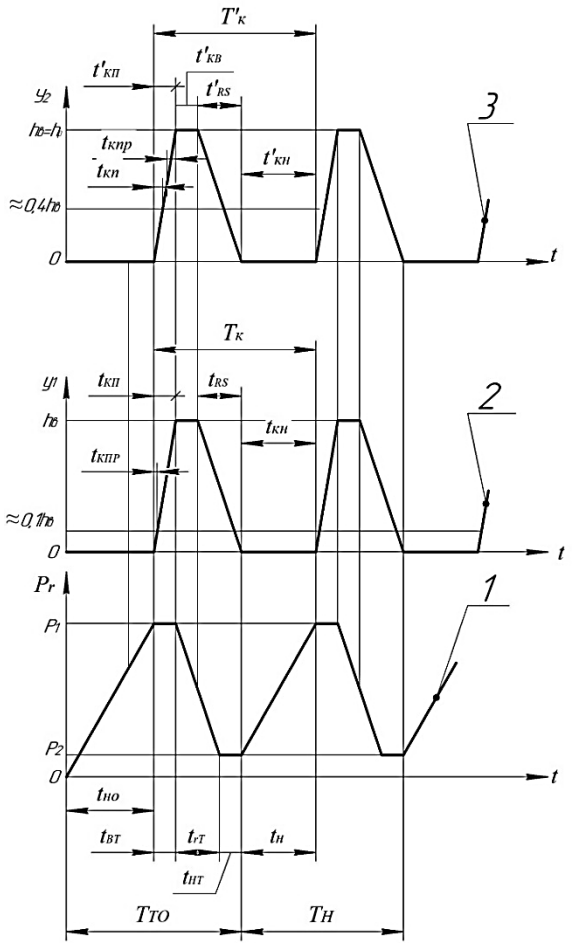

Figure 2 – Approximate cyclogram of the operating cycle for a small-sized hydraulic pulse vibrator with a built-in valve PPG: 1 – energy carrier pressure change in the pressure cavity A (Figure 1) of the vibrator; 2 – movement curve of the vibrator plunger; 3 – movement curve of the valve bushing

Also, in formula (6), t_{rT} – the reverse time of pressure reduction in the pressure cavity during the opening of the PPG shut-off elements, s; t_{HT} – holding time of the energy carrier pressure p_2 in the pressure cavity A, s; t_{kn} – travel time of plunger 8 (locking element of the first level of PPG sealing) to the full straight stroke $h_b = h_p$ (full opening of the PPG), s; $t_{kb} = t'_{kb}$ – time of standing time of the plunger 8 together with the valve sleeve 9 in the extreme position of the straight stroke (fully open PPG), s; $t_{RS} = t'_{RS}$ – time of the return stroke of the plunger 8 and valve sleeve 9 on the working stroke h_b, s; t_{kh} – time of the plunger movement in the initial (closed) position, s; t'_{kh} – time of the valve sleeve movement to the $h_s = 0.4h_b$ gap, s.

The above-mentioned time intervals t_j are functions of the system's dynamic parameters (mass, stiffness, pressure force) and are determined by numerically solving the differential equations presented in the next section, which are based on the d'Alembert principle. Although equation (6) represents the general structure of the oscillation period T_K as the sum of time intervals, inertial effects are

therefore fully taken into account in determining each dynamic component.

According to the approximate cyclogram (Figure 2) of the vibrator's operating cycle, the plunger's forward stroke is carried out relative to the pressure pulse with a phase shift $t_{kh} = t_H$, and the beginning of the direct movement of the valve sleeve 9 is shifted relative to the direct stroke of the plunger 8 by time $t_{knp} = h_b - h_s = 0.6h_b$.

The time t_H of the energy carrier pressure build-up in the pressure cavity A (Figure 1) can be estimated with sufficient accuracy for design calculations by the following dependence:

$$t_H = \frac{W_0 \Delta p}{\kappa Q_H}, \quad (7)$$

where $\Delta p = (p_1 - p_2)$ – amplitude of the pressure pulse, Pa; W_0 – the initial volume of the pressure cavity A of the vibrator hydraulic system, m^3; Q_H – hydraulic pump's flow rate, m^3/s.

Notably, the parameter W_0 includes the volume of the hydraulic pressure line, for example, a high-pressure hose from a hydraulic pumping station.

According to formula (7), the increase in the pressure of the energy carrier in the pressure cavity A occurs according to a linear law for a case of, e.g., Q_H = const, κ = const, and W_0 = const. Actually, the hydraulic pump's flow rate Q_H, which is diverted to a volume that varies within certain limits due to energy losses in the PPG and hydraulic equipment of the hydraulic pumping station, is affected by overflow, for example, into the drain cavity. The volume W_0 is also not constant due to the addition (or subtraction) of additional volumes due to the movement of the PPG locking and power links and the vibrator, except κ = const in the absence of dissolved air and impurities of other substances (except oil) in the energy carrier.

The relationship between the pressure pulse amplitude Δp at time t, the flow rate Q_H, the effective bulk modulus κ, and the initial volume W_0 is nonlinear and can take the form of either a convex or a concave curve. In Figure 2, this mode illustrates the established cycle, where the period T_H corresponds to a frequency of 55 Hz, and the initial T_{I0} pulse demonstrates the transient start-up process. For the specified parameters, the system has entered a stable self-oscillating mode at approximately 55 Hz.

4 Results

4.1 Dynamic models

Compared to the mass m_2 of the valve sleeve 9 (Figure 1), the mass m_1 of the plunger 8 is significantly higher. Also, the mass m_2 is a separate dynamic element (Figure 2) that moves along the path approximating $0.4h_b$ (maximum $0.5h_b$) during the straight stroke of the plunger 8 for a relatively short time $t_{knp} < t'_{kn}$. During this time, $t'_{kn} = (t_{kp} - t_{knp})$, the plunger 8 completes a straight stroke and the valve sleeve 9 moves as one ($m_{1\Sigma} = m_1 + m_2$) with the plunger 8 during the time $t_{knb} + t'_{kb} + t'_{RS}$ (here $t'_{kb} = t_{kb}$, and $t'_{RS} = t_{RS}$). This specificity of the dynamics of the second stage of sealing of the PPG (sleeve-valve 9) allows, to simplify the dynamic and mathematical model of the vibrator, not to consider a separate differential equation of mass m_2 movement both during the forward and reverse strokes, and to take into account the peculiarities of the dynamics of the second stage of sealing of the PPG of the vibrator under the conditions of unambiguity (boundary conditions) of the mathematical model of the vibrator.

To obtain the highest possible frequencies of pressure pulses and vibrations of the executive links of hydraulic pulse machines and devices, their initial volume W_0 of pressure cavities is minimized, that makes it possible to neglect the influence of the mass of the energy carrier in the pressure cavities of their hydraulic system, which is small compared to the movements of the mass of the rigid links of the VD or VIM, on the dynamics of these machines or devices.

Under this assumption, the hydraulic link (HL) in the dynamic model of the vibrator can be considered a Kelvin–Voigt body [20], consisting of massless elastic k_0 and dissipative c_0 elements connected in parallel. The HL in the form of Kelvin–Voigt corresponds to the elastic-viscous concentrated model of the energy carrier, which takes into account both elastic and dissipative (viscous) properties of the working fluid (energy carrier), and the HL obeys all the laws of hydrostatics and hydrodynamics.

The use of the Kelvin–Voigt model with concentrated parameters to describe the HL in our study is based on the specific design and operating ranges of the vibrator under consideration. At a frequency of 150 Hz, the wavelength is approximately L = 8 – 9 m. Since the actual channels and supply hoses of the vibrator are significantly shorter than these values (less than 1.5 m), the dynamic processes in the system can be treated as processes with concentrated parameters without any significant loss of accuracy. The compressibility of the fluid in our model is accounted for by the reduced modulus of elasticity κ and the *HL* stiffness k_{0r}.

The influence of dissolved air and temperature does indeed alter the physical parameters (density, viscosity); however, in the theoretical model, it can be used as an "effective" elastic modulus that already incorporates these factors as average values for steady-state operation. The Kelvin–Voigt model is chosen to account for internal friction in the fluid (dissipative elements), which is critical for small-scale systems due to the "scale effect," in which viscous resistance increases with decreasing cross-sectional area.

To form an HL in the form of a Kelvin–Voigt body, all the HLs and hydraulic channels of the pressure cavity A of the vibrator are reduced to an average HL (pipe) with an average cross-sectional area, m^2:

$$A_0 = \frac{\sum_{i=1}^{N} A_i l_i}{L_0}, \quad (8)$$

where N – number of elements; A_i – area of the i-th element of the hydraulic channel, m^2; l_i – length of the i-th element of the HL, m; L_0 – the total length, m:

$$L_0 = \sum_{i=1}^{N} l_i. \quad (9)$$

In this averaged HL, the energy carrier (considered as a droplet Newtonian fluid) can deform under pressure, according to Hooke's law:

$$\Delta p_r = p_r - p_{dp} = \kappa \varepsilon_W = \kappa \cdot \frac{\Delta W}{W_{0\Sigma}}, \quad (10)$$

where Δp_r – pressure drop in the pressure cavity A of the vibrator hydraulic system, Pa; p_r – current energy carrier pressure in the pressure cavity, Pa; p_{dp} – pressure in the drain cavity of the vibrator hydraulic system, Pa; ε_W – relative volumetric deformation of the energy carrier in the pressure cavity A due to compression in the averaged energy carrier hydroline; $W_{0\Sigma} = A_0 \cdot L_0 = \text{const}$ – initial volume of the pressure cavity, m^3; ΔW – change in the initial volume, m^3;

Notably, pressure p_{dp} in the drain cavity of the vibrator hydraulic system is usually neglected ($p_{dp} = 0$).

Since the volume W_0 is the volume of energy carrier in a pipe with a cross-sectional area $A_0 = \text{const}$, the compressed volume and the volumetric deformation are as follows:

$$\Delta W = A_0 \cdot x_{0r}; \quad (11)$$

$$\varepsilon_W = \frac{A_0 \cdot x_{0r}}{W_{0\Sigma}}, \quad (12)$$

where x_{0r} – variable linear deformation of the energy carrier in the internal HL of the pressure cavity of the vibrator hydraulic system, m.

Since the HL is a liquid rod with length L_0 and cross-sectional area A_0, the initial stiffness k_{0r} of the HL can be calculated by the following formula:

$$k_{0r} = \frac{\kappa A_0^2}{W_{0\Sigma}}. \quad (13)$$

In the averaged HL, the current pressure p_r can be determined after substitution of dependencies (11)–(13) into equation (10), where

$$p_r = \frac{k_{0r} \cdot x_{0r}}{A_0}. \quad (14)$$

The HL interacts with the moving masses m_1 and m_1, the vibrator. In this regard, the transfer ratio from the HL to the i-th moving link is as follows:

$$U_{0i} = \left(\frac{A_i}{A_0}\right)^2, \quad (15)$$

where A_i – the i-th cross-sectional area, m^2.

During the working process, the initial stiffness k_{0r} of the HL changes due to the addition (or subtraction) to the initial volume W_0 of the pressure cavity A (Figure 1) of additional volumes of ergonomic fluid consumed for the movement of the plunger 8 and the valve sleeve 9 during their forward and reverse strokes, as well as for the actual compression of the energy carrier under the influence of its high pressure.

Theoretical and experimental studies of hydro-pulse VD and VIM have established in [1, 11–15, 18, 19] that these additional volumes of energy carrier are small compared to W_0 and can be neglected, and $k_{0r} = \text{const}$ throughout the entire operating cycle of the vibrator, which greatly simplifies its dynamic and mathematical models.

The stiffness k_{0r} of the HL can be reduced to any cross-sectional area of the moving link of the vibrator according to the following relationship:

$$k_{0i} = U_{0i} \cdot k_{0r}, \quad (16)$$

where $i = \overline{1, N}$ – serial number of the i-th moving link of the vibrator.

Similarly, the linear strain x_{0r} and its velocity $\dot{x}_{0r}$ can also be reduced to any cross-sectional area of the moving link of the vibrator as follows [15]:

$$x_{Ai} = \frac{x_{0r}}{\sqrt{U_{0i}}}; \quad (17)$$

$$\dot{x}_{Ai} = \frac{\dot{x}_{0r}}{\sqrt{U_{0i}}}. \quad (18)$$

The viscous drag force F_{A0} of the HL (internal friction in the energy carrier) during its deformation according to Newton's law for droplet liquids:

$$F_{A0} = C_0 \dot{x}_{0r}, \quad (19)$$

where $C_0 = \pi \mu_e d_0^2/4 \approx 0.785 \mu_e d_0^2$ – coefficient of viscous resistance during deformation of the HL; $d_0 = 2\sqrt{A_0/\pi} \approx 1.13\sqrt{A_0}$ – hydraulic diameter, m.

The i-th force F_{Ai} can also be converted to the cross-sectional area of any moving link of the vibrator using the following formula:

$$F_{Ai} = C_0(\dot{x}_{0r} \pm \dot{y}_{0r})\sqrt[4]{U_{0i}}, \quad (20)$$

$\dot{y}_i$ – the current speed of movement of the first vibrator link, m/s.

Notably, the "+" sign is set when the movement of the vibrator link increases the deformation x_{0r}, and "–" when it decreases.

The operating cycle of a real hydraulic-pulse vibrator (like a hydraulic-pulse vibrator or hydraulic-pulse vibrating machine) is determined by numerous dynamic parameters that may also vary randomly. Taking into account the influence of as many of these parameters as possible on the vibrator's dynamics (e.g., in a mathematical model of the vibrator) would greatly complicate this model and create insurmountable mathematical difficulties for its analysis and investigation. Therefore, to reduce the complexity of the dynamic and mathematical modeling of the hydro-pulse vibrator under investigation, it is advisable, in addition to those previously outlined, to adopt further reasonable assumptions (structure of assumptions):

– the thermodynamic heat transfer process in the hydraulic system of a vibrator, during the steady-state phase of its operating cycle (starting from the second pressure change pulses p_r, and displacements y_1, y_2) is isothermal;

– the physical parameters of the working fluid within the operating cycle change insignificantly, which allows for considering $\kappa = \text{const}$, $\rho_e = \text{const}$; $v_e = \text{const}$ (or dynamic viscosity of a liquid carrier $\mu_e = \text{const}$);

– hydrodynamic forces during the opening and closing of the first (plunger 8) and second (valve sleeve 9) sealing stages of the PPG (Figure 1) are small compared to the

driving forces and resistance forces and are not considered in the initial differential equations of the vibrator's mathematical model;

– wave processes in the hydraulic lines of the vibrator's hydraulic system are absent due to the short length of the hydraulic channels and lines in this system;

– the constant weight force of plunger 8 and the technological object affected by the vibrator, in the case of its vertical orientation, is accounted for in the force F_T;

– compared with the energy carrier flows during the opening and closing of the vibrator's PPG, energy losses through the seals of the vibrator's moving and stationary parts are absent or very small;

– it can be assumed that the flow rate of the working fluid through the open gaps in the first and second sealing stages of the PPG is quadratic, and that the flow coefficients through these gaps are constant values;

– only fluid friction occurs in the guide bushings of the plunger 8 and the valve sleeve 9 (Figure 1);

– simulation starts from a stationary state, considering initial boundary conditions (at $t = 0$: $y = \dot{y} = 0$, and $p = 0$) to capture the transient start-up process and the build-up of the initial stiffness of the HL;

Mineral oil (type IGP-30) has been selected for the simulation, the characteristics of which have been adapted to the operating conditions: temperature $T = (40 \pm 5)$ °C, taking into account the following physicochemical parameters of the working fluid:

– dynamic viscosity $\mu_e = 0.026$ Pa·s, and density $\rho_e = 870$ kg/m^3 were used to calculate the viscous resistance coefficient c_0 using equation (19);

– the effective modulus of elasticity $\kappa = 1.4 \cdot 10^9$ Pa corresponds to the presence of 2–3 % undissolved air, which is typical for industrial hydraulic systems and significantly reduces the theoretical stiffness of pure oil.

Based on the adopted framework of assumptions and an indicative cyclogram of the working process (Figure 2), the idealized dynamic model of the vibrator with absolutely rigid plunger 8 and valve sleeve 9 is presented in Figure 3 in the form of a moving mass $m_{1\Sigma} = (m_1 + m_2)$ loaded with positional elastic forces, dissipative and constant technological resistance forces, which interacts with the HL through the transfer ratios $U_{01(02)}$ (forward mass movement) and $U_{02(01)}$ (reverse mass movement).

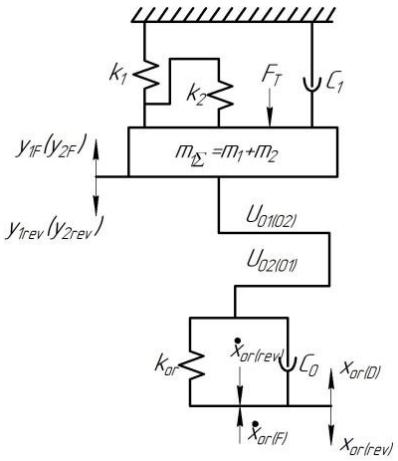

Figure 3 – Dynamic model of a small-sized hydraulic pulse vibrator with a built-in valve PPG

In addition to the previously mentioned values of the vibrator parameters and its operating cycle, Figure 3 shows the following: C_1 – the consolidated coefficient of viscous friction during the movement of mass m_1 (plunger 8 together with the valve sleeve 9), N·s/m; y_{1F} (y_{2F}), and y_{1rev} (y_{2rev}) – current coordinates of movement of the plunger 8 and the valve sleeve 9, respectively, during the direct and their reverse strokes, m; $\uparrow \dot{x}_{or(n)}$ – direction of the HL deformation rate during the forward and reverse (↓) strokes of the mass $m_{1\Sigma}$; $\dot{x}_{0r(F)}$, $\dot{x}_{0r(D)}$ – directions of the HL deformation during the forward and reverse strokes of the mass $m_{1\Sigma}$, respectively, m/s.

Under the assumptions made when calculating the mass m_1 (4), the stiffness k_1 of the slotted spring 13 is recommended to be calculated by the simplified formula [18]:

$$k_1 = \frac{1.035Ea^4}{nR^3}, \qquad (21)$$

where $E = 2.15 \cdot 10^{11}$ N/m^2 – Young's modulus of the slotted spring's material.

The stiffness k_2 of the twisted spring 10 is determined by the standard approach [21].

To simplify the process of constructing a mathematical model of the vibrator based on its dynamic model (Figure 3), it can be divided an initial dynamic model [14] into two simple models of the forward (Figure 4 a) and reverse (Figure 4 b) mass $m_{1\Sigma}$ movements, using the principle of partitioning, by reducing the HL to mass $m_{1\Sigma}$.

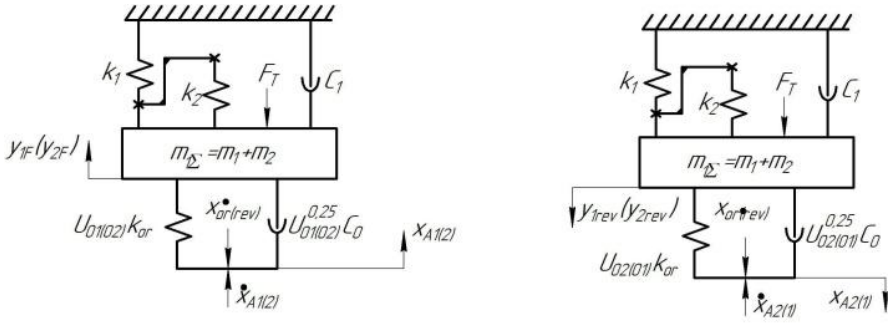

a b

Figure 4 – Simplified dynamic models of the forward (a) and reverse (b) mass $m_{1\Sigma}$ movements

The twisted spring 10 (Figure 1) interacts with the fixed hydraulic cylinder sleeve 2 through the movable plunger 8 and slotted spring 13. This interaction is shown in the dynamic models (Figures 3, 4) as a Z-shaped rigid rod.

4.2 Mathematical modeling results

The mathematical model of the vibrator consists of differential equations of mass $m_{1\Sigma}$ movement during its forward and reverse strokes, equations of energy consumption during these strokes during the working cycle, and uniqueness conditions that set the limits for changing the deformation x_{0r} of the HL, the gear ratio from $U_{01(02)}$ to $U_{02(01)}$ and vice versa, and the movement of the plunger 8 (Figure 1).

The differential equations of mass $m_{1\Sigma}$ motion are based on the d'Alembert principle for strokes:

1) direct ($x_{01} \geq x_{0r(F)} \geq x_{02}$):

$$\begin{gathered} m_{1\Sigma} \cdot \ddot{y}_{1F} = U_{01(02)} k_{0r}\left[x_{A1(2)} - y_{1F}\right] - \\ -k_1(y_{1F} + y_{01}) + [k_2(y^*_{1F} - y_{02})]^{**} - \\ -c_1\dot{y}_{1F} - F_T - \sqrt[4]{U_{01(02)}} \cdot c_0\left(\dot{x}_{A1(2)} - \dot{y}_{1F}\right); \end{gathered} \tag{22}$$

2) reverse ($x_{02} \geq x_{0r(rev)} \geq 0$):

$$\begin{gathered} m_{1\Sigma} \cdot \ddot{y}_{1rev} = k_1(y_{01} + h_b - y_{1rev}) - \\ -[k_2(y^*_{02} - y_{1rev})]^{**} + F_T - \\ -U_{02(01)} k_{0r}\left[x_{A1(2)} - (h_b - y_{1rev}) - c_1\dot{y}_{1F} - \right. \\ \left. -\sqrt[4]{U_{02(01)}} \cdot c_0\left(\dot{x}_{A2(1)} - \dot{y}_{1rev}\right)\right], \end{gathered} \tag{23}$$

where where $x_{01} = \frac{p_1 A_0}{k_{0r}}$, $x_{02} = \frac{p_2 A_0}{k_{0r}} = \frac{x_{01}\sqrt{U_{21}}}{k_{0r}}$ – the boundary deformations of the HL, corresponding to the pressure of "opening" p_1 and "closing" p_2 of the PPG, m; $U_{21} = \left(\frac{A_1}{A_2}\right)^2 = \left(\frac{d_1}{d_2}\right)^4$ – the internal transmission ratio between the first and second sealing stages of the PPG (for $0 < y_{1F} < h_{gap} \approx \left[0.4h_b - U_{01(02)}\right] = \left(\frac{A_1}{A_0}\right)^2$: $m_{1\Sigma} = m_1$; on the interval of mass m_1 movement $y^*_{1F} \leq 0.4h_b$, the force equals $[k_2(y^*_{1F} - y_{02})]^{**}$, and for the mass m_2, the forces is fixed; for $h_s \leq y_{1F} \leq \left[h_b - U_{01(02)}\right] = \left(\frac{A_2}{A_0}\right)^2$, $m_{1\Sigma} = (m_1 + m_2)$ plunger 8 and valve sleeve 9 move as one unit (Figure 1), and at the interval $h_s \leq y_{1F} \leq h_b$, the force of the spring 10 is compensated by the dynamic pressure of the energy carrier with a reduced pre-load ($y_{02} - y_{1F}$), which allows for neglecting the force $[k_2(y^*_{1F} - y_{02})]^{**}$ from the equation of motion (22) on this interval; $x_{A1(2)} = \frac{x_{0r(D)}}{\sqrt{U_{01(02)}}}$, $\dot{x}_{A1(2)} = \frac{\dot{x}_{0r(D)}}{\sqrt{U_{01(02)}}}$ are determined based on the formulas (17), (18) for the above changes y_{1F} and $U_{01(02)}$); for $0 \leq y_{1rev} \leq 0.4h_b$, $m_{1\Sigma} = (m_1 + m_2)$ and $U_{21} = \left(\frac{A_1}{A_0}\right)^2$, as well as for $0.4h_b \leq y_{1rev} \leq h_b$, $m_{1\Sigma} = m_1$, and also $U_{21} = \left(\frac{A_1}{A_0}\right)^2$ (due to the inertial acceleration of the plunger 8 on the way back, it is advisable to omit the closing area of the valve sleeve 9 on the cyclogram for simplification); $x_{A1(2)} = \frac{x_{0r(s)}}{\sqrt{U_{02(01)}}}$, $\dot{x}_{A1(2)} = \frac{\dot{x}_{0r(s)}}{\sqrt{U_{02(01)}}}$; $\dot{y}_{1F}$, $\ddot{y}_{1F}$, $\dot{y}_{1rv}$, and $\ddot{y}_{1rev}$ – the current velocity and mass acceleration $m_{1\Sigma}$ (m_1 and m_2) during its forward and reverse strokes; $x_{A1(2)}$, $x_{A2(1)}$, $\dot{x}_{A1(2)}$, and $\dot{x}_{A2(1)}$ – deformations and deformation rates of the HL are reduced to the corresponding cross-sectional areas of the first and second sealing stages of the vibrator's PPG (plunger 8 and valve sleeve 9).

For the system of differential equations (22) and (23) to have a solution, it is necessary to add the equations that determine the change in the deformation x_{0r} of the HL during the operating cycle of the vibrator. This change x_{0r} is caused by the energy carrier consumption for its initial deformation (20), movement of the plunger 8 and the valve sleeve 9 (Figure 1), and the energy carrier flow into the corresponding cavities (mainly from the pressure A to the drain C cavity) of the PPG vibrator.

Nonlinear differential equations of the types (22) and (21) are usually solved and studied numerically [21] using various software, such as MATLAB, in which the time step is the main explicit argument. This feature of numerical methods allows the law of deformation x_{0r} change of the HL vibrator for mass $m_{1\Sigma}$ movements to be written in the form of simple laws:

1) direct:

$$x_{0r(F)} = x_{01} - \frac{Q_{\Sigma lF}}{A_0} \cdot t_i; \tag{24}$$

2) reverse:

$$x_{0r(rev)} = x_{02} \pm \frac{Q_{\Sigma lrev}}{A_0} \cdot t_i^{/}, \tag{25}$$

where $Q_{\Sigma lF}$, $Q_{\Sigma lrev}$ – the flow rate of energy carrier through the hydraulic lines and the open gap of the PPG (the first and second stages of sealing of the PPG), which corresponds to certain movements of the moving links of the vibrator on the way of the direct (l_F) and reverse (l_{rev}) mass movements $m_{1\Sigma}$; t_i, $t_i^{/}$ – current time of change of a certain state l_F or l_{rev}) of energy consumption in $Q_{\Sigma lF}$ or $Q_{\Sigma lrev}$ (Figure 2).

To determine the energy consumption $Q_{\Sigma lF}$ and $Q_{\Sigma lrev}$ at different time intervals of the approximate cyclogram of the vibrator operating cycle (Figure 2), the methodology given in [15] can be applied, for example, for the strokes of the plunger 8 and the valve sleeve 9 (masses $m_{1\Sigma}$):

a) direct for the time intervals and movements of the locking elements of the first and second sealing levels of the PPG:

1) $y_{1F} = y_{2F} = 0$; $x_{0r(F)} = \frac{\int_0^{t_H} Q_H dt}{A_0} = x_{01} \equiv x_{0max}$;

2) $0 < y_{1F} \leq 0.1h_b, y_{2F} = 0$; $x_{0r(F)} = x_{01} - Q_{\Sigma 1lF} t_{knp}$; $Q_{\Sigma 1lF} = Q_H = \dot{y}_{1F} \cdot A_1$;

3) $0.1h_b < y_{1F} \leq 0.4h_b$, $0 < y_{2F} \leq 0.4h_b$; $x_{0r(F)} = x_{01} - Q_{\Sigma 2lF}(t_{kn} - t_{knp}) = x_{01} - Q_{\Sigma 2lF} \cdot t_{knH}$; $Q_{\Sigma 2lF} = Q_H = \dot{y}_{1F} \cdot A_1 + \dot{y}_{2F} \cdot (A_2 - A_1)$;

4) $y_{1F} = y_{2F}$, $0.4h_b \leq y_{1F} \leq h_b$, $0.4h_b \leq y_{2F} \leq h_b$, $\dot{y}_{1F} = \dot{y}_{2F}$; $x_{0r(F)} = x_{01} - Q_{\Sigma 3lF} \cdot (t_{knb} + t_{kb}^{/})$; $Q_{\Sigma slF} = Q_H + y_{2F} \cdot A_2 = Q_{HD}$,

where Q_{HD} – total energy carrier flow rate through the open slots of the first and second shut-off elements of the PPG – valve elements of the plunger 8 and the valve sleeve 9 (Figure 1), which consists of a variable part (the first part of dependence (26):

$$Q_{HD} = \frac{1}{2}\xi_H \pi d_2 [(y_{2F} - 0.4h_b) + |y_{2F} - 0.4h_b|] \times \times \sqrt{\frac{2k_{0r}x_{01}}{\rho_e A_0}} + \xi_H \pi d_2 h_b \sqrt{\frac{2k_{0r}x_{01}}{\rho_e A_0}} \times \times \sqrt{x_{01}\left(1 - \sqrt{U_{21}}\right) + \frac{k_1 h_b}{k_{0r}\sqrt{U_{02}}}}. \quad (26)$$

It is determined by the time interval t_{knp}, mass $m_{1\Sigma} = (m_1 + m_2)$ movement along the path $0.4h_b \le y_{2F} \le h_b$ (or $0.4h_b \le y_{01} \le h_b$) at a constant HL deformation x_{01} = const (the second part of formula (26) for time $t'_{KB} = t_{KB}$ and a fully open slit of the PPG with a cross-sectional area $A_{gap}^{max} = \pi d_2 h_b$ of the HL deformation difference $x_{01} - x_{02} = \Delta x_{0r}(1 - \sqrt{U_{21}}) + \frac{k_1 k_{0r} h_b}{\sqrt{U_{02}}}$ (corresponds to $\Delta p = p_1 - p_2$); ξ_H– flow coefficient through A_{gap} the PPG (assumed to be ξ_H = const);

b) inverse at the displacement intervals $y_{1rev} = y_{2rev}$ ($0 \le y_{2rev} \le h_b$, and $0 \le y_{1rev} \le h_b$ at changes in the directions of mass $m_{1\Sigma}$ movements and deformation x_{0r} of the HL (Figure 4 b) during the time $t_{RS} = t'_{RS}$:

1) $0 < y_{2rev} \le h_b$, $0 < y_{1rev} \le h_b$;

$x_{0r(rev)} = x_{02} + Q_{\Sigma 1lrev} \cdot t'_{rev}$;

$Q_{\Sigma 1lrev} = Q_H + \dot{y}_{2rev} \cdot A_2 = Q_{Hrev}$,

where Q_{Hrev} – flow consumption due A_{gap} to the return stroke of the mass $m_{1\Sigma} = (m_1 + m_2)$:

$$Q_{Hrev} = \frac{1}{2}\xi_H \pi d_2 [(h_b - y_{2rev}) + |h_b - y_{2rev}|] \times \times \sqrt{\frac{2k_{0r}}{\rho_e A_0}\left[x_{01}\sqrt{U_{21}} + \frac{k_1 h_b}{k_{0r}\sqrt{U_{02}}}\right]}; \quad (27)$$

2) $y_{1rev} = y_{2rev} = h_b$; $t_{kn} = t'_{kn} - t_{knp}$;

$x_{0r(rev)} = \frac{\int_0^{t_H} Q_H dt}{A_0} = x_{01}$.

The conditional passage of the PPG vibrator should be of such a size as to ensure the passage of the maximum flow of energy carrier at the permissible speed [18]. The formula for determining the maximum possible flow of the energy carrier passing through A_{gap}^{max} can be obtained by analyzing dependencies (26) and (27). After simple algebraic transformations from dependencies (26) and (27), it can be found:

$$Q_{H\Sigma}^{max} = 2.404\pi d_2 \xi_H h_b \sqrt{\frac{k_{0r}x_{01} + 2k_1 h_b \sqrt{U_{02}}}{\rho_e A_0}}. \quad (28)$$

Differential equations (22) and (23), to determine the i-th eigenfrequency ω_i, characterizing the HL system – the moving links of the vibrator (plunger 8 and valve sleeve 9); it is advisable to present it in a form that emphasizes the oscillatory nature of this dynamic system.

Dividing the right and left sides of equations (22) and (23) by $m_{1\Sigma}$, after algebraic transformations, it can be obtained for the strokes:

1) direct ($x_{01} \ge x_{0r(D)} > x_{02}$):

$$\ddot{y}_{1F} + 2\beta_{1F}\dot{y}_{1F} + \omega_{\Sigma 1(F)}^2 y_{1F} + + \omega_{01}^2\left(y_{01} - \delta y_{02}^*\right) + \frac{F_T}{m_{1\Sigma}} = = -\omega_p^2\sqrt{U_{02(01)}} \cdot x_{or(F)}; \quad (29)$$

2) inverse ($x_{02} \ge x_{0r(rev)} \ge 0$):

$$\ddot{y}_{1rev} + 2\beta_{1rev}\dot{y}_{1rev} + \omega_{\Sigma 1(rev)}^2 y_{1rev} + + \omega_{01}^2\left(y_{01} + h_в - \delta y_{02}^*\right) + \frac{F_T}{m_{1\Sigma}} = = -\omega_p^2\sqrt{U_{02(01)}} \cdot x_{0r(rev)}, \quad (30)$$

where β_{1F}, β_{1rev} – damping coefficients during mass movement, on its forward and reverse strokes, s^{-1}:

$$\beta_{1F} = \frac{c_1 + c_0 \cdot \sqrt[4]{U_{02(01)}} \cdot \left[\frac{\dot{x}_{A1(2)}}{\dot{y}_{1F}} - 1\right]}{2m_{1\Sigma}};$$

$$\beta_{1rev} = \frac{c_1 + c_0 \cdot \sqrt[4]{U_{02(01)}} \cdot \left[\frac{\dot{x}_{A2(1)}}{\dot{y}_{1rev}} - 1\right]}{2m_{1\Sigma}}.$$

Equations (29), (30) include the following eigen- and partial frequencies:

$$\omega_p = \sqrt{\frac{k_{or}}{m_{1\Sigma}}}; \omega_{01} = \sqrt{\frac{k_1}{m_{1\Sigma}}}; \omega_{02} = \sqrt{\frac{k_2}{m_{1\Sigma}}} = \sqrt{\delta};$$

$$\omega_{\Sigma 1(F)} = \sqrt{U_{01(02)}\omega_p^2 + (1+\delta)\omega_{01}^2};$$

$$\omega_{\Sigma 1(rev)} = \sqrt{U_{02(01)}\omega_p^2 + (1+\delta)\omega_{01}^2},$$

where δ – stiffness ratio.

To facilitate the analysis of the mathematical model of the vibrator and simplify the appearance of equations (29) and (30), the free terms can be excluded from these equations of the mass $m_{1\Sigma}$ motion by replacing the variables y_{1F} and y_{1rev} with new variables z_{1F} and z_{1rev}, which do not change the nature and dynamics of mass motion $m_{1\Sigma}$:

$$\begin{cases} z_{1F} = y_{1F} + \omega_{\Sigma 1(F)}^2\left[\omega_1^2(y_{01} - 8y_{02}^*) + \frac{F_T}{m_{1\Sigma}}\right]; \\ z_{1rev} = y_{1rev} + \omega_{\Sigma 1(rev)}^2\left[\omega_1^2(y_{01} + h_в - 8y_{02}^*) + \frac{F_T}{m_{1\Sigma}}\right]. \end{cases} \quad (31)$$

With the new variables, the differential equations of motion of the mass $m_{1\Sigma}$ for its movements will take the form:

1) direct ($x_{01} \ge x_{0r(F)} > x_{02}$):

$$\ddot{z}_{1F} + 2\beta_{1F}\dot{z}_{1F} + \omega_{\Sigma 1(F)}^2 z_{1F} = \omega_p^2\sqrt{U_{01(02)}} \cdot x_{0r(F)}; \quad (32)$$

2) reverse ($x_{02} \ge x_{0r(rev)} \ge 0$):

$$\ddot{z}_{1rev} + 2\beta_{1rev} + \omega_{\Sigma 1(rev)}^2 z_{1rev} = -\omega_p^2\sqrt{U_{01(02)}} \cdot x_{0r(rev)}. \quad (33)$$

At different stages of movement (including during the forward and reverse strokes) of the plunger 8 and the valve sleeve 9 (Figure 1), the natural circular frequencies $\omega_{\Sigma 1(F)}$

and the vibrator – HL system change, since the transfer ratio $U_{01(02)}$ or $U_{02(01)}$ and $m_{1\Sigma}$ from $m_{1\Sigma} = m_1$ to $m_{1\Sigma} = (m_1 + m_2)$, in addition to the valve sleeve 9 (the mass m_2 moves independently during the forward stroke at a distance $h_{rev} = 0.4h_b$).

Changes in the gear ratios $U_{01(02)}$ and $U_{02(01)}$ and $m_{1\Sigma}$ are indicated in the decoding of the values in differential equations (22) and (23).

The natural circular frequency, for example $\omega_{\Sigma1(F)}$, can be expressed in terms of the total stiffness $k_{\Sigma1(F)}$of the HL vibrator system:

$$k_{\Sigma1(F)} = m_{\Sigma1}\omega^2_{\Sigma1(F)} = U_{01(02)}k_{or} + (1 + \delta)k_1, \quad (34)$$

which is sometimes advisable to use in the design calculations of such hydraulic pulse vibrators. Formula (34) for design calculations can be simplified if considering $\delta = \frac{k_2}{k_1} << 1$, then:

$$k_{\Sigma1(F)} \approx U_{01(02)}k_{or} + k_1, \quad (35)$$

and during the working cycle of the vibrator can take on two values:

$$k_{\Sigma1min} = U_{01}k_{0r} + k_1 = \left(\frac{d_1}{d_0}\right)^4 k_{0r} + k_1; \quad (36)$$

$$k_{\Sigma1max} = U_{02}k_{0r} + k_2 = \left(\frac{d_1}{d_0}\right)^4 k_{0r} + k_1. \quad (37)$$

By extracting from the formulas (36) and (37), a relationship between $k_{\Sigma1min}$ and $k_{\Sigma1max}$ can be established:

$$k_{\Sigma1min} = k_{\Sigma1max} - k_{0r} \cdot \frac{d_2^4 - d_1^4}{d_0^4} = k_{\Sigma1max} - k_{0r} \cdot \frac{A_2^2 - A_1^2}{A_0^2} = k_{\Sigma1max} - \kappa \cdot \frac{A_2^2 - A_1^2}{W_0}. \quad (38)$$

If considering the difference $\Delta k_{\Sigma1} = (\Delta k_{\Sigma1max} - \Delta k_{\Sigma1min})$ to k_{0r}, it can be obtained:

$$\delta_{k_{\Sigma1}} = \frac{\Delta k_{\Sigma1}}{k_{0r}} = \frac{d_2^4 - d_1^4}{d_0^4} = \frac{A_2^2 - A_1^2}{A_0^2} = const. \quad (39)$$

This dependence shows that the change in the relative total stiffness of the vibrator – HL system from the maximum to the minimum (or vice versa) values is a constant value and is determined only by the geometric parameters of the first and second stages of sealing of the PPG and the average HL hydroline.

To some extent, formulas (36)–(39) can be used to estimate the range of changes in the natural total circular frequencies in hydraulic pulse devices and vibrators, which mainly determine the dynamics of these hydraulic pulse machines.

The differential equations (32) and (33), together with the energy flow equations (24)–(28) and the constraints on the mass $m_{1\Sigma}$ movement and deformation x_{0r} of the HL, forms a mathematical model of a small-sized hydro-pulse vibrator with a valve PPG.

As noted above, it is possible to study mathematical models of mechanical systems, including hydraulic pulse VD and VIM, using various applied computer programs, consistently solving the differential equations of motion of *MS* slats for different parameter values using the numerical methods included in these programs.

To provide a detailed analysis of the developed mathematical model, a Python simulation code was developed to visualize the workflow. The Python script uses numerical integration (Euler's method for systems of differential equations). Figure 5 shows a flowchart of the numerical modeling algorithm implemented in Python. Figure 6 shows the results of simulations in the Google Colab software environment.

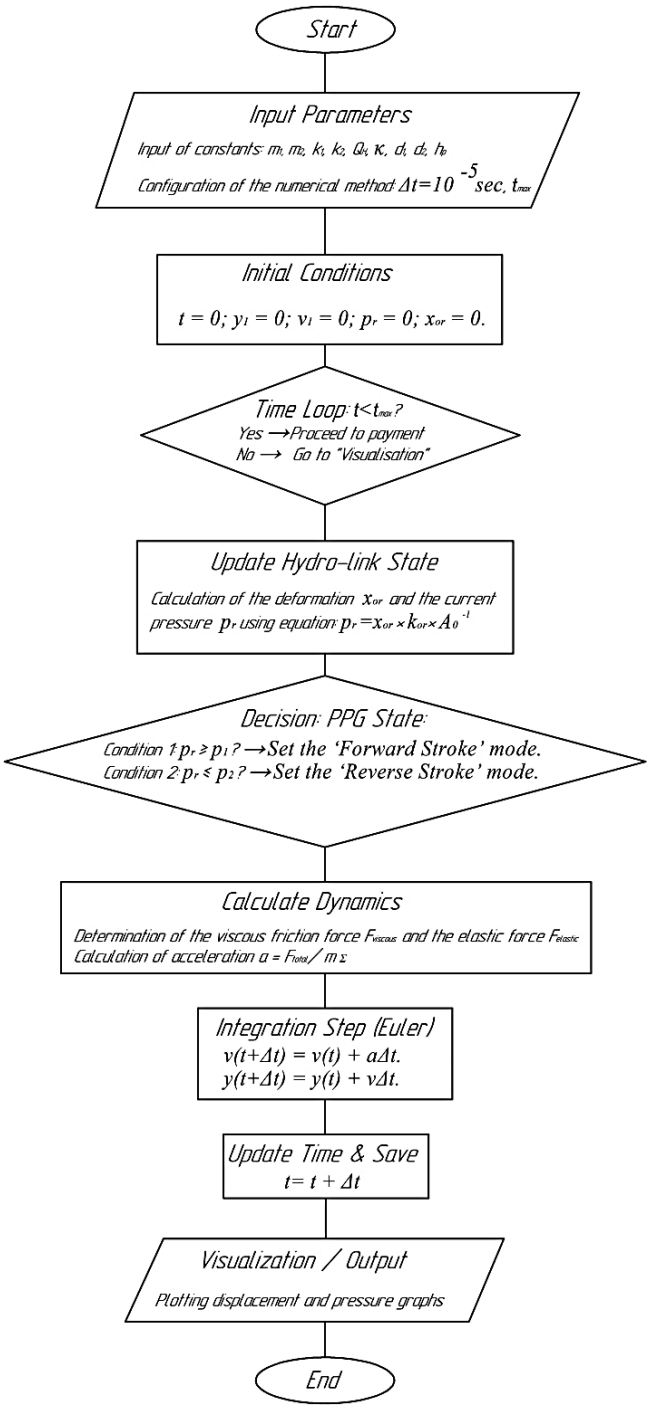

Figure 5 – Block diagrams of numerical modeling algorithms

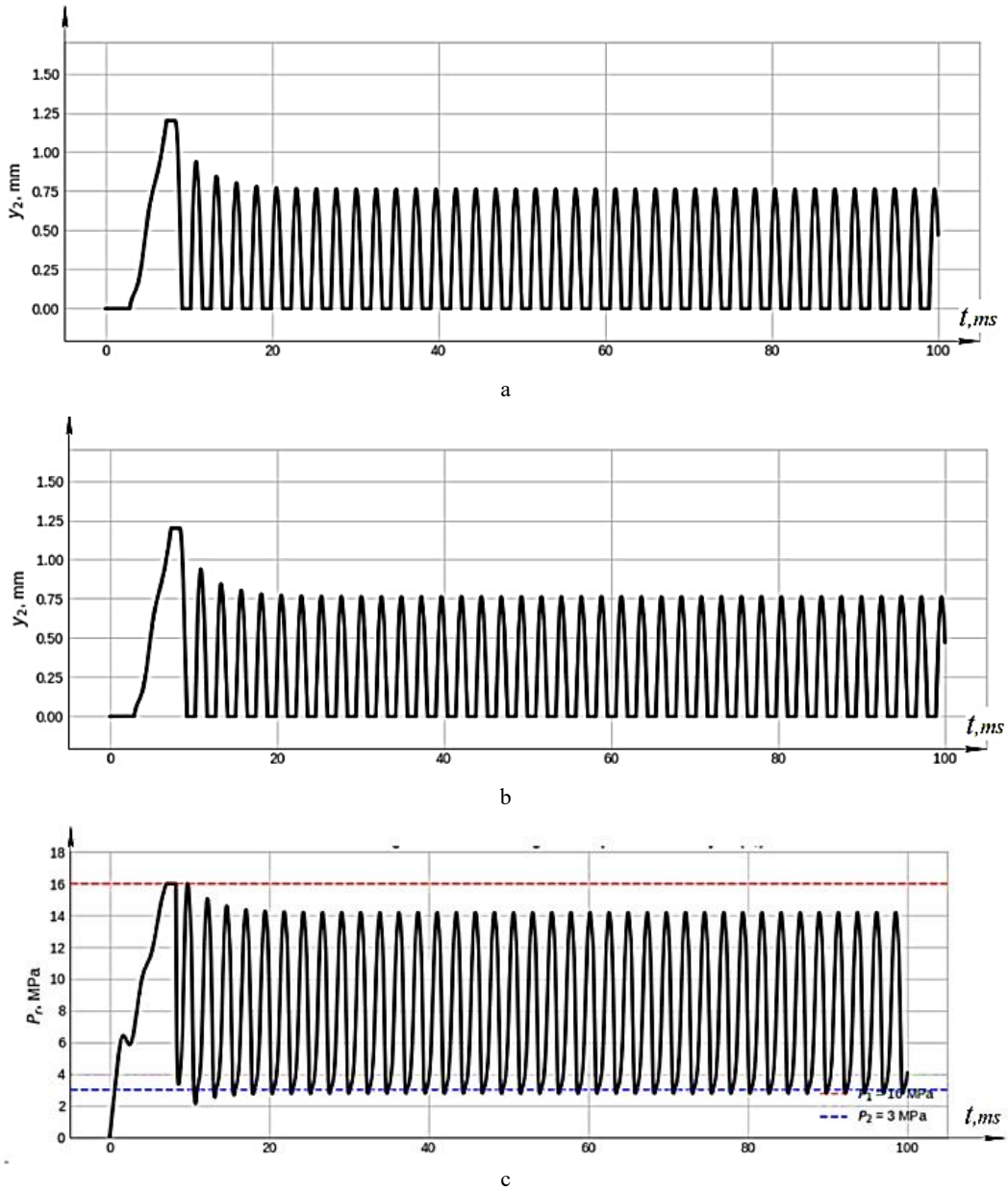

Figure 6 – Numerical simulation results: a – movement curve of the valve bushing 9 PPG vibrator; b – movement curve of the vibrator plunger 8; c – curve of energy carrier pressure change in the pressure cavity *A* of the vibrator (Figure 1)

Euler's method was applied to solve the system of nonlinear differential equations (22), (23), (32), and (33) and the energy balance equations (24)–(28). This method was chosen for its effectiveness in systems with frequent switching events, which are characteristic of valve PPG operation during the transition from the closed to the open state. The simulation time step was set $\Delta t = 1 \cdot 10^{-5}$ s (0.01 ms). This relatively small step was chosen, given the vibrator's maximum frequency (up to 150 Hz), which provides over 600 calculation points per oscillation period, ensuring solution stability and correct recording of valve actuation moments. The simulation was implemented in Python (using the NumPy library for matrix calculations and Matplotlib for visualization) in the Google Colab environment.

4.3 Accuracy and stability of the numerical solution

The Euler method was used to solve the system of differential equations (22)–(33). Since the system is stiff due to discontinuous functions at the PPG valve actuation points (p_1 and p_2), stability was ensured by selecting a small integration step $\Delta t = 1.0 \cdot 10^{-5}$ s. This value satisfies the Courant condition for this oscillatory system, with a natural frequency of approximately 55 Hz. With this step size, one oscillation period is described by over 1800 calculation points, which eliminates the risk of computational instability;

– a double-check procedure verified the accuracy of the method with a reduced step size $\Delta t = 5 \cdot 10^{-6}$ s;

– it was established that the relative error in calculating the amplitude of the plunger displacement y_1, and the peak pressure pr does not exceed 0.05 %;

– the convergence of the solution is confirmed by the stability of the phase shift and the preservation of the system's energy balance over 100 simulation cycles;

– the stability of the solution is also supported by the use of the Kelvin–Voigt model, where the presence of a dissipative element (coefficient c_0) naturally dampens the high-frequency numerical oscillations that might arise in a purely elastic model.

The analysis showed that spring stiffness primarily affects the return speed and the dwell time of the plunger in its end positions. Stiffer springs shorten the return cycle, shifting the system into the high-frequency range, but may slightly reduce the amplitude due to the rapid valve closure.

Simulation confirmed that the amplitude depends on the valve opening time and the mass inertia. At the specified parameters (2.0 mm), the system demonstrates stability; however, at extreme frequencies (above 120 Hz), a natural "damping" of the amplitude is observed due to the hydraulic circuit's viscous resistance. It has been established that the working fluid's flow rate is the primary parameter for frequency control. An increase in leads to a proportional reduction in the pressure rise time t_H. This allows the frequency to be smoothly varied within the range of 15–150 Hz.

5 Discussion

The developed mathematical and dynamic models of the small-dimension hydropulse vibrator with a built-in valve-type PPG provide a comprehensive understanding of the highly nonlinear interaction between fluid dynamics and mechanical moving parts. Unlike traditional simplified "relay" models [11–13], the proposed approach represents the HL as a Kelvin–Voigt body. This explicitly accounts for both the elastic compressibility (bulk modulus) and the viscous dissipation of the energy carrier, which is critically important for small-dimension hydraulic systems where the "scaling effect" becomes prominent, as previously highlighted in [10].

The obtained mathematical dependencies, coupled with numerical simulation using the operational parameters of a standard gear pump, confirmed the auto-oscillatory nature of the system. The model accurately predicts the phase shift between the pressure rise in the working cavity and the mechanical displacement of the plunger (mass m_1). The inertia of the combined masses $m_{1\Sigma}$ that causes a phase shift and the HL's compliance. Recent studies in digital hydraulics and high-frequency actuation by Zhu et al. [8] and Hua et al. [17] highlight the challenge of controlling the pressure-rise rate dp/dt in compact valve chambers. The proposed model elegantly addresses this by introducing the dynamic gap h_s and the time delay t_{kpr} before the valve sleeve (mass m_2) opens. This parametric self-regulation ensures a stable "dwell" phase (approximately 15 % of the forward stroke time) followed by a sharp pressure drop, which is highly desirable for generating shock-vibration impulses without the need for complex external electronic controls.

Furthermore, the integration of lumped-parameter modeling in this research aligns with the latest trends in adaptive control systems, as in the simulation modeling of adaptive hydraulic drives discussed by Veselovska et al. [2]. By adjusting parameters such as the initial spring pre-load y_{01} and pump flow rate Q_H, the system's operational frequency can be seamlessly tuned within a broad range (typically 15–150 Hz, with the simulated base configuration operating stably around 55–65 Hz).

The developed mathematical framework lays the groundwork for several advanced analytical and practical applications:

1. The model can be utilized to perform a multi-criteria optimization of the vibrator's design parameters (e.g., k_1, k_2, d_1, d_2, and h_s). Target functions could be set to maximize the impact energy (for vibro-cutting or surface hardening) while minimizing the hydraulic shock loads on the pump and pipeline infrastructure.

2. The proposed system of differential equations (32), (33), and energy balance equations is computationally efficient. It can be embedded into a real-time "Digital Twin" of the technological machine, allowing predictive maintenance and real-time adjustment of hydraulic parameters to maintain resonance, similar to the steady-state modes investigated by Filimonikhin [6].

3. For further refinement, it is proposed to validate the lumped Kelvin–Voigt fluid model against advanced 3D CFD coupled with FSI analysis. This will provide deeper insights into the local cavitation effects and flow coefficients during the highly transient opening phase of the PPG.

The proposed design of a compact hydraulic pulse vibrator with a built-in parametric valve PPG exhibits significant commercial and technological potential. Its main advantage is its high power density, combined with mechanical simplicity (no rotary spools or fragile electronic solenoids).

Experimental validation of the model is planned as the next stage of the research, using the laboratory test rig developed, which is equipped with high-frequency pressure sensors and laser displacement sensors to compare real-world waveforms with numerical modeling results. Future experiments will focus on comparing real-world pressure and displacement waveforms with numerical simulation results obtained in Python to refine the values of the viscous resistance coefficient c_0 and the effective elastic modulus. Particular attention will be paid to the operation of the vibrator in the high-frequency range (100–150 Hz) to confirm the parametric stability of the natural vibrations predicted by our mathematical model.

Nonlinearity is a crucial issue for hydraulic impulse systems. A balance between computational complexity and physical accuracy can be struck during model development, based on the following considerations:

– the model accounts for nonlinear flow characteristics, recognizing that the flow of the working fluid through the open slits of the PPG is a time-dependent variable that

depends on the position of the control elements and the deformation of the HL;

– the effect of hydraulic shock is partially accounted for through a dynamic model of the HL as a Kelvin–Voigt body, which describes elastic pressure oscillations.

– since the length of the pressure line in our compact vibrator is minimal, pressure losses along its length (linear losses) are negligible compared to local losses in the valve mechanism.

The primary objective of the model was to determine the parametric frequency range (15–150 Hz) and the conditions for the stability of self-oscillations. As shown by similar studies, for preliminary design and vibrator frequency-tuning tasks, models with concentrated parameters provide the necessary engineering accuracy.

6 Conclusions

Based on the results of a detailed analysis of the vibrator's operating cycle, an indicative cyclogram of the workflow implemented during the operation of the vibrator was constructed, which established the relationship between changes in the pressure of the energy carrier in the pressure cavity of the vibrator's hydraulic system and the movements of the plunger and the valve sleeve during certain phases of the vibrator's operating cycle.

The relationship between the maximum and minimum values of the total stiffness of the vibrator - hydraulic line system has been established, which shows that the change in the relative total stiffness of the vibrator - hydraulic link system (from the minimum to the maximum value or vice versa) is a constant value and is determined by the primary geometric parameters.

According to the results of research in the Google Colab software environment, for the current rigid parameters (for the study, the following were accepted: pump type QH-32, stroke of the executive body (plunger) – 2.0 mm, maximum operating pressure of the pressure pulse generator – 16 MPa), the vibrator will operate stably in the range of about 55 Hz. By changing the pump, opening/closing pressure, or reducing the plunger stroke, this design can be easily brought into the high-frequency range of 100–150 Hz.

It has been confirmed that the operating frequency range of a hydraulic pulse vibrator of this design is not a single fixed number – it is parametric and depends on the settings of the hydraulic system. In general, for small-sized hydraulic pulse vibrators with a built-in valve pressure pulse generator, the operating frequency range is usually from 15 Hz to 150 Hz.

It has also been established that the stiffness of the main springs determines the speed of reverse movement (when the pressure drops to 3 MPa) and the dwell time. The stiffer the springs, the faster the system returns to its initial position, reducing the overall cycle time. By selecting the spring's stiffness, it is possible to shape the pulse to be most effective for the corresponding technological process.

Analysis of the results from the study of the developed mathematical model in the Google Colab software environment showed a phase shift between the pressure peak and the plunger's maximum displacement. This is explained by the inertia and viscous friction in the hydraulic link, which confirms the selection of the Kelvin–Voigt model.

The eigenfrequencies of the vibrator were determined, and the change in the system's total stiffness during the vibrator's operating cycle was analyzed. It was also shown that the relative total stiffness of the system depends only on the geometric parameters of the first and second stages of sealing of the pressure pulse generator and the average hydraulic diameter.

The results of this study correlate well with those of experimental studies on similar hydraulic pulse drives for vibrating and vibro-impact machines.

The study of the developed mathematical model enables optimizing the design, implementing various structural modifications of the vibrator based on the features of the technological process, and developing a methodology for the design calculation of the proposed new vibrator.

Nomenclature

a – jumper's edge, m;

A – chamber;

A_0 – average cross-sectional area of the hydraulic line, m^2;

A_1, A_2 – cross-sectional areas of the pressure pulse generator sealing stages, m^2;

A_i – area of the i-th element of the channel, m^2;

B – intermediate chamber;

"b" – hole;

C – drainage cavity;

c_0 – coefficient of viscous resistance during hydraulic link deformation, N·s/m;

C_1 – consolidated coefficient of viscous friction of the moving masses, N·s/m;

CFD – computational fluid dynamics;

D – cavity;

d_1, d_2 – average diameters of the 1st and 2nd pressure pulse generator sealing stages, m;

d_3, d_4, d_5 – structural diameters of the sleeve and plunger, m;

E – Young's modulus of the slotted spring's material, N/m^2;

F – forward index;

F_{A0} – viscous drag force, N;

FSI – fluid-structure interaction;

F_T – vertical placement of the vibrator, m;

F_{T0} – the initial force under technological influence of the plunger rod, N;

F_{Tmax} – maximum resistance force, N;

$g = 9.81$ m/s^2 – gravity acceleration;

h_b – the negative overlap (opening) of the second stage of the sealing system, m;

HL – hydraulic line;

h_p – full stroke value of the pressure pulse generator, m;

HPD – hydraulic pulse drive;

h_{rev} – reverse stroke of the plunger, m;
h_s – dynamic gap (negative overlap) of the 2nd pressure pulse generator sealing stage, m;
i – link number;
j – time interval number;
k_0 – coefficient of stiffness during hydraulic link deformation, N/m;
k_{0r} – initial stiffness of the hydraulic link, N/m;
k_1, k_2 – stiffness of the slotted and twisted springs, N/m;
L – wavelength, m;
L_0 – average length of the hydraulic line, m;
l_i – length of the i-th element of the hydraulic line, m;
m_1, m_2 – masses of the plunger and the valve sleeve, kg;
$m_{1\Sigma} = m_1 + m_2$ – combined moving mass, kg;
"*max*" – maximum index;
m_i – mass of the i-th element, kg;
"*min*" – minimum index;
N – number of elements;
n – number of jumpers;
p – pressure, Pa;
Δp – amplitude of the pressure pulse, Pa;
p_1, p_2 – opening and closing pressure levels of the pressure pulse generator, Pa;
PPG – pressure pulse generator;
p_c – contact pressure, Pa;
p_{dp} – pressure in the drain cavity of the vibrator hydraulic system, Pa;
p_r – energy carrier pressure in the pressure cavity, Pa;
Δp_r – pressure drop in the pressure cavity of the vibrator hydraulic system, Pa;
Q_H – flow rate of the hydraulic pump, m^3/s;
Q_{HD} – total flow carrier flow rate, m^3/s;
Q_{Hrev} – flow consumption in the return stroke, m^3/s;
$Q_{\Sigma lF}$, $Q_{\Sigma lrev}$ – the flow rates of energy carrier, m^3/s;
R – average radius of the slotted spring, m;
"*rev*" reverse index;
T – temperature, °C;
t – time, s;
Δt – numerical integration time step, s;
t_{BT} – the time of pressure reduction in the pressure cavity during the opening of the PPG shut-off elements, s;
t_H – pressure build-up time in the pressure cavity, s;
t_{HT} – holding time of the energy carrier pressure in the pressure cavity, s;
t_i – i-th time interval, s;
T_K, T'_K – periods of changes in the current coordinates of the plunger and valve sleeve displacement, s;
t_{kb}, t'_{kb} – time of standing time of the plunger and the valve sleeve in the straight stroke's extreme position, s;
t_{kh} – time of the plunger movement in the initial (closed) position, s;
t'_{kh} – time of the valve sleeve movement to the 40 % gap distance, s;
t_{kn} – travel time of plunger to the full straight stroke, s;
t_{kp}, t_{rev} – duration of the forward and reverse strokes, s;
t_{RS}, t'_{RS} – time of the return stroke of the plunger and the valve sleeve on the working stroke, s;
t_{rT} – the reverse time of pressure reduction in the pressure cavity during the shut-off elements opening, s;
T_T – period of pressure change, s;
T_{T0} – initial time of pressure change, s;
$U_{01(02)}$, $U_{02(01)}$ – transfer ratio for the direct and transfer movements, respectively;
U_{0i} – transfer ratio from the hydraulic link to the i-th moving link;
VD – vibration drive;
VIM – vibration-impact machine;
$W_{0\Sigma}$ – initial volume of the pressure cavity, m^3;
x_{01}, x_{02} – the boundary deformations for opening and closing modes, m;
x_{0r} – linear deformation of the energy carrier in the hydraulic line, m;
$\dot{x}_{0r(F)}$, $\dot{x}_{0r(D)}$ – directions of the deformation during the forward and reverse strokes, m/s;
x_{Ar} – averaged linear displacement, m;
$\dot{x}_{Ar}$ – averaged linear velocity, m/s;
y – displacement, m;
$\dot{y}$ – velocity, m/s;
y_{01}, y_{02} – preliminary deformation (pre-load) of the slotted and twisted springs, m;
y_1, y_2 – current coordinates of the plunger and valve sleeve displacement, m;
z_{1F}, z_{1rev} – dynamic displacements, m;
β_{1F}, β_{1rev} – damping coefficients during mass movement on its forward and reverse strokes, s^{-1};
δ – stiffness ratio;
ε_W – relative volumetric deformation of energy carrier;
κ – effective bulk modulus of the energy carrier, Pa;
μ_e – dynamic viscosity of the carrier, Pa·s;
ν_e – kinematic viscosity of the carrier, m^2/s;
ρ – material density, kg/m^3;
ρ_e – carrier density, kg/m^3;
"Σ" – the total sum index;
ξ_H – flow coefficient;
ω_i – i-th eigenfrequency, rad/s.

Conflicts of Interest

The authors declare no conflicts of interest.

References

1. Obertyukh, R., Slabkyi, A., Petrov, O., Bakalets, D. (2024). Substantiation of the methodology for calculating the design of a small-sized hydraulic pulse vibrator. *Vibroengineering Procedia*, Vol. 56, pp. 22–28. https://doi.org/10.21595/vp.2024.24512
2. Veselovska, N.R., Rutkevych, V.S., Shargorodskiy, S.A., Yaropud, V.M., Kupchuk, I.M. (2025). Simulation modeling of the adaptive system for hydraulic drives of a stalk forage separator. *Journal of Engineering Sciences (Ukraine)*, Vol. 12(1), pp. F8–F17. https://doi.org/10.21272/jes.2025.12(1).f2

3. Mardare, I., Tiţa, I, Pelin, R.I. (2016). Researches regarding a pressure pulse generator as a segment of model for a weighing in motion system. *IOP Conference Series: Materials Science and Engineering*, Vol. 147, 012060. https://doi.org/10.1088/1757-899X/147/1/012060
4. Xuan, J., Wang, S., Liu, H. (2018). Design and control of a hydraulic composite actuator for vibration simulation. *Advances in Mechanical Engineering*, Vol. 10(5). https://doi.org/10.1177/1687814018773809
5. Kachur, O., Korendiy, V. (2023). Dynamic behavior of vibratory screening conveyor equipped with crank-type exciter. *In: V. Ivanov, I. Pavlenko, O. Liaposhchenko, J. Machado, M. Edl (Eds.). Advances in Design, Simulation and Manufacturing VI. DSMIE 2023*, pp. 44–53. Lecture Notes in Mechanical Engineering, Springer, Cham, Switzerland. https://doi.org/10.1007/978-3-031-32774-2_5
6. Filimonikhin, G., Yatsun, V., Matsui, A., Kondratets, V., Pirogov, V. (2022). Selection and research of stability of the steady state motions of a single-mass resonance vibromating machine working on the Somerfeld effect. *Eastern-European Journal of Enterprise Technologies*, Vol. 3(7(117)), pp. 68–76. https://doi.org/10.15587/1729-4061.2022.259567
7. Gursky, V., Krot, P., Korendiy, V., Zimroz, R. (2022). Dynamic analysis of an enhanced multi-frequency inertial exciter for industrial vibrating machines. *Machines*, Vol. 10(2), 130. https://doi.org/10.3390/machines10020130
8. Zhu, Z., Li, H., Wang, Y., Chen, X. (2022). Study on the characteristics of a new hydraulic pulse generator for drilling. *Journal of Petroleum Science and Engineering*, Vol. 208(D), 109724. https://doi.org/10.1016/j.petrol.2021.109724
9. Gutierrez, D.A., Garcia-Bravo, J.M., Reid, A.R., Newell, B.A., McPherson, P., French, M. (2020). Design and modelling of a 90-degree ball valve with a linear pressure drop. *International Journal of Fluid Power*, Vol. 21(1), pp. 1–26. https://doi.org/10.13052/ijfp1439-9776.2111
10. Al-Obaidi, A.R., Alhamid, J. (2025). Experimental and simulation analyses of the hydraulic complex internal flow characteristics in an axial pump based on varying frequency vibration ranges technique. *International Journal on Interactive Design and Manufacturing*, Vol. 19, pp. 3661–3681. https://doi.org/10.1007/s12008-024-02012-9
11. Iskovych-Lototskyi, R.D. (2006). *Fundamentals of the Theory of Calculation and Development of Processes and Equipment for Vibro-Impact Pressing*. Universum, Vinnytsia, Ukraine.
12. Manzhilevskyy, O.D. (2019). Analysis of hydraulic vibration drive machine for vibration abrasive processing. *Przegląd Elektrotechniczny*, Vol. 1(4), pp. 95–99. https://doi.org/10.15199/48.2019.04.16
13. Sevostianov I.V. (2021). *Processes and Equipment for Vibro-Impact Filtration of Wet Dispersed Media*. Vinnytsia National Agrarian University, Vinnytsia, Ukraine.
14. Obertyukh, R., Slabkyi, A., Petrov, O., Kudrash, V. (2021). Mathematical modeling of the device for radial vibroturning. *In: V. Tonkonogyi, V. Ivanov, J. Trojanowska, G. Oborskyi, A. Grabchenko, I. Pavlenko, M. Edl, I. Kuric, P. Dasic (Eds.). Advanced Manufacturing Processes II. InterPartner 2020*, pp. 566–576. Lecture Notes in Mechanical Engineering, Springer, Cham, Switzerland. https://doi.org/10.1007/978-3-030-68014-5_55
15. Obertyukh, R., Slabkyi A., Polishchuk, L., Povstianoi, O., Kumargazhanova, S., Satymbekov, M. (2022). Dynamic and mathematical models of the hydroimpulsive vibro-cutting device with a pressure pulse generator built into the ring spring. *Informatyka, Automatyka, Pomiary w Gospodarce i Ochronie Środowiska*, Vol. 12(3), pp. 54–58. https://doi.org/10.35784/iapgos.3049
16. Al-Obaidi, A.R., Alwatban, A. (2025). Investigation of hydraulic transient flow and dynamic response performance of axial pump based on novel vibration signals characteristics and numerical analyses. *Alexandria Engineering Journal*, Vol. 125, pp. 104–126. https://doi.org/10.1016/j.aej.2025.04.012
17. Hua, S., Liu, S., Qiu, Z., Wang, X., Zhang, X., Zhang, H. (2024). The design and experimental research on a high-frequency rotary directional valve. *Processes*, Vol. 12(11), 2600. https://doi.org/10.3390/pr12112600
18. Virnuk, M., Iskovich-Lototsky, R., Veselovskaya, N. (2004). *Vibration and Vibration Processes and Machines in Foundry Production*. Vinnytsia National Agrarian University, Vinnytsia, Ukraine.
19. Bulíček, M., Málek, J., Rajagopal, K.R. (2012). On Kelvin-Voigt model and its generalizations. *Evolution Equations & Control Theory*, Vol. 1(1), pp. 17–42. https://doi.org/10.3934/eect.2012.1.17
20. Kubrak, M., Malesińska, A., Kodura, A., Urbanowicz, K., Stosiak, M. (2021). Hydraulic transients in viscoelastic pipeline system with sudden cross-section changes. *Energies*, Vol. 14(14), 4071. https://doi.org/10.3390/en14144071
21. Xue, D., Pan, F. (2024). *MATLAB and Simulink in Action*. Springer, Singapore. https://doi.org/10.1007/978-981-99-1176-9_13